ChemPhysChem

Research Article
doi.org/10.1002/cphc.202500306

Chemistry Europe
European Chemical Societies Publishing

www.chemphyschem.org

Proton Exchange Between 3,6-Di-Tert-Butyl-2-Hydroxyphenoxyl and Dicarboxylic Acids Studied by Electron Spin Resonance Spectroscopy and Density Functional Theory Calculations

Sergey Nikolskiy,* Farida Abilkanova, Alfiya Kurmanova, and Rakhim Rakhimov

The reaction of intermolecular proton exchange between the spin probe 3,6-di-tert-butyl-2-hydroxyphenoxyl and some dicarboxylic acids, such as oxalic, maleic, succinic, and adipic, is studied. The experimental spectra of the radical with acids are recorded using dynamic electron spin resonance (ESR) spectroscopy. The studies are carried out at different temperatures in toluene. The rate constants of intermolecular proton exchange are determined by modeling the ESR spectra of the radical using equations based on the modified Bloch equations and the four-site jump model. It follows from the kinetic data that with an increase in the acid's carbon chain, the reaction rate slightly decreases, and the value of the activation barrier of the reaction increases. Analysis of the kinetic data using the Bell–Limbach model made it possible to calculate the components of the reaction's energy barrier. Quantum chemical calculations of the studied systems using the density functional theory B3LYP and the 6-31+G(d,p) basis set show that the proton exchange mechanism is a cooperative two-proton exchange. Calculations using the XMCQDPT/SA(4)-CASSCF(1,4)/6-31+G(d,p) method also show that excited states do not affect this process. This methodology can be used to determine the rate constants of intra- and intermolecular processes involving various OH- and NH-acids.

1. Introduction

The proton directly reacts in various environments and chemical and biological systems. Recently, interest in studying complexes and reactions involving hydrogen has increased significantly. This is evidenced by numerous publications.[1–10] To explain the mechanisms of the processes, theoretical approximations are used, in which this process is considered from various points of view, starting from the transfer of a hydrogen atom and ending with multiple interpretations of proton and electron transfer, including proton-coupled electron transfer.[11–15] The use of various physical methods for studying the dynamics of such processes is usually limited, first, by the objects of study for the corresponding method, and second, by the time range of the method used. The most widely used method for these purposes is dynamic nuclear magnetic resonance spectroscopy, which allows studying processes in the time range of $\approx 10-10^5\,s^{-1}$.[16–20] Dynamic electron spin resonance (ESR) spectroscopy allows significant expansion of the time range from $\approx 10^6$ to $10^9\,s^{-1}$.

One of the problems in obtaining experimental kinetic data is the search for a suitable model system in which intramolecular and intermolecular hydrogen transfer processes take place, which can be monitored using dynamic ESR spectroscopy. One such system is stable semiquinone radicals, which can be used as acid-type spin probes.[21–24] The use of nitroxyl radicals as spin probes, despite their good solubility in any medium, is limited by their lower sensitivity to the acid–base properties of the medium.[25–27] Previously, we obtained the kinetic parameters of intermolecular proton transfer from 4-triphenylmethyl-6-tert-butyl-3-chloro-2-hydroxyphenoxyl to various nitroxyl radicals, such as 2,2,3,5,5-pentamethyl-3-imidazoline-N-oxyl. The corresponding characteristics of the process were obtained from the spectral changes in the semiquinone radical.[28] A "sensitive" hydroxyl group in the radicals allows it to study acid–base systems in nonaqueous media. Semiquinone radicals can participate in proton transfer reactions with organic bases and proton exchange reactions with NH and OH acids. The use of semiquinone radicals allows us to evaluate the kinetic basicity of a number of organic bases and the protolytic ability of some NH and OH acids.[29–33] A significant disadvantage of oxyphenoxyl radicals is their insolubility in aqueous solutions. This paper presents ESR spectroscopic studies of the protolytic capacity of some dicarboxylic acids of various structures, such as oxalic, maleic, succinic, and adipic acids, in toluene medium, using a 3,6-di-tert-butyl-2-hydroxyphenoxyl spin probe, as well as a quantum chemical interpretation of the obtained ESR

S. Nikolskiy, F. Abilkanova, A. Kurmanova
Department of Physical and Analytical Chemistry
Karaganda Buketov University
st. Universitetskaya, 28, 100024 Karaganda, Kazakhstan
E-mail: sergeynikolsky@mail.ru

S. Nikolskiy
Department of Physical and Inorganic Chemistry
Altai State University
Barnaul 656049, Russia

R. Rakhimov
Department of Chemistry & Center for Materials Research
Norfolk State University
700 Park Avenue, Norfolk, Virginiya 23504, USA

Supporting information for this article is available on the WWW under https://doi.org/10.1002/cphc.202500306

spectroscopic data. A particular interest in the protolytic reactivity of dicarboxylic acids is associated with the presence of two identical acid centers in the molecules; moreover, the thermodynamic acidity of the acids in question is known to be higher than that of monocarboxylic acids of similar structure. This fact is explained by the mutual influence of carboxyl groups, facilitating dissociation associated with the spatial interaction of electrons of two carboxyl groups, characteristic of dicarboxylic acids. Significantly, due to the presence of two COOH groups, these compounds exhibit unique coordination properties capable of chelating reagents.[34–38]

2. Results and Discussion

2.1. Experimental Data

The ESR spectrum of 3,6-di-tert-butyl-2-hydroxyphenoxyl in the absence of intermolecular interactions exhibits a triplet of doublets. Each component of the triplet ($a_H = 0.392$ mT) arises from the hyperfine interaction between the unpaired electron and the ring protons, and further splits into a doublet ($a_H^{OH} = 0.162$ mT) due to coupling with the hydroxyl group proton. This latter splitting remains virtually constant over a wide temperature range. The spectral pattern changes upon heating the radical–acid system. **Figure 1** presents the ESR spectra of the studied radical–oxalic acid system obtained in toluene at various temperatures. As seen from the spectra, an increase in temperature leads to a characteristic broadening of the hyperfine structure lines of the radical and a decrease in the hyperfine coupling constant of the hydroxyl proton. The observed broadening of the doublet lines of the radical and the reduction in hydroxyl splitting are attributed to intermolecular proton exchange (IPE) between the radical and the acid, as described in detail in references.[29–33] The small magnitude of the spectral changes may indicate that this process occurs relatively "slowly" on the ESR timescale. Nevertheless, despite the apparent lack of pronounced spectral variations, the applied software enables the evaluation of the kinetic parameters of the process.[39]

The IPE between 3,6-di-tert-butyl-2-hydroxyphenoxyl and carboxylic acids, taking into account tautomeric transformations of the radical, can be represented as shown in **Scheme 1**.

The scheme represents a four-site jump model, in which the radical forms differ in the position of the hydrogen atom and its spin state. IPE occurs within complexes via hydrogen bonding. It can be described by processes of intramolecular tautomerism within the radical (A ⇄ B or C ⇄ D), as well as IPE between the radical and the acid (A ⇄ C) ⇄ (B ⇄ D).

ESR spectra of the radical for all studied acids were obtained in a saturated toluene solution of the respective acid. A factor influencing the kinetic parameters of IPE is the low concentration of the acids in toluene, which is due to their limited solubility in this solvent. The low acid concentrations allowed us to exclude the influence of processes, such as radical solvation and acid self-association on the IPE. From the observed spectral changes, the kinetic parameters of IPE were determined for each acid. The rate

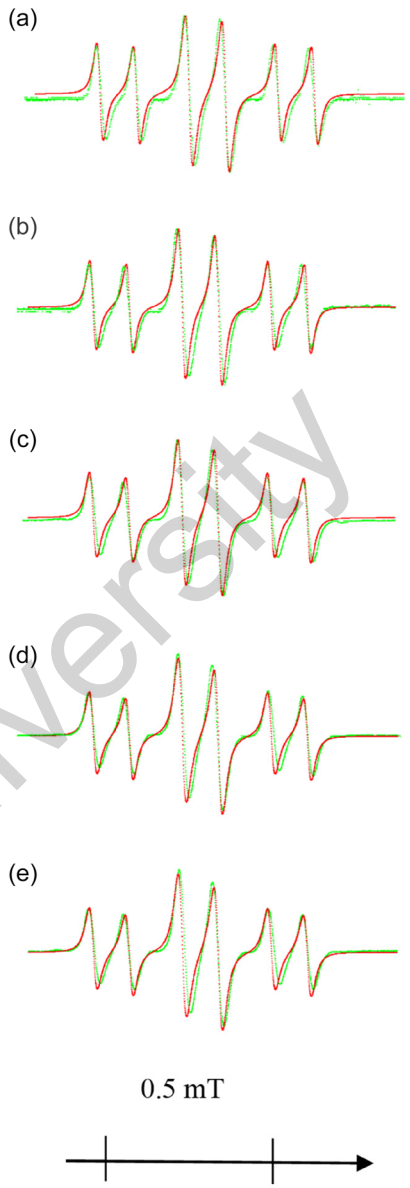

Figure 1. Experimental (green) and simulated (red) ESR spectra of the spin probe 3,6-di-tert-butyl-2-hydroxyphenoxyl in the presence of oxalic acid at selected temperatures: a) 295 K, b) 303 K, c) 321 K, d) 331 K, and e) 341 K. Concentration of OxA = 0.007 M in toluene. Linewidth = 0.035 mT. Change in the constant from 1.62 to 1.48.

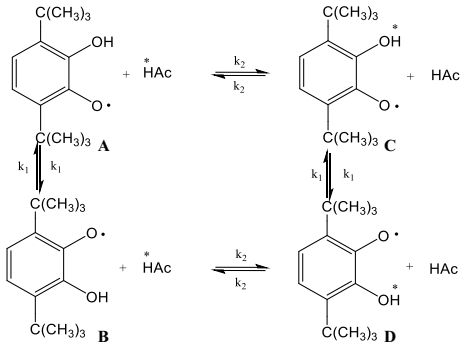

Scheme 1. Scheme of IPE of the 3,6-di-tert-butyl-2-hydroxyphenoxyl with acids.

constant of proton exchange between the radical and the acid was calculated as

$$k_{exch} = \frac{1}{4}\frac{v_{exch}}{[Acid]},\ l \cdot mol^{-1}s^{-1} \quad (1)$$

where v_{exch} is obtained from the model ESR spectra, the coefficient $\frac{1}{4}$ accounts for the probability of a change in the proton spin due to the reaction (Scheme 1), [Acid] - acid concentration.

Table 1 presents the kinetic parameters of the studied acids. The Arrhenius plot shows a linear correlation between $\ln k_{exch}$ and $\frac{1}{T}$ (**Figure 2**).

Error bars on the Eyring plots represent the standard error (SE) of the mean, indicating the precision of the mean value estimate and the range in which the real value is likely to lie with 95% probability (95% CI = × ± 1.96·SE).

As seen from the obtained data, the rate constant of IPE between the radical and dicarboxylic acids is on the order of $\approx 10^7\ s^{-1}$. This value decreases with increasing carbon chain length of the acid. At the same time, an increase in the activation barrier of the reaction is observed across the series of acids studied.

A distinctive feature of this process within the four-site jump model is that IPE occurs only if the rate of intramolecular tautomerism (A ⇄ B and C ⇄ D) is on the order of $\approx 10^9\ s^{-1}$. The pre-exponential factor ($\approx 10^{10}\ s^{-1}$) also shows a tendency to increase along the homologous series of acids.

Table 1. Kinetic parameters of the fast IPE reactions between radical and acids in toluene solution.

Acid	k_{exch} [293 K] [$l \cdot mol^{-1}s^{-1}$]	k^0_{exch} [$l \cdot mol^{-1}s^{-1}$]	E_a [$kJ \cdot mol^{-1}$]	pK_a [Reference]
Oxalic	$(2.1 \pm 0.3) \cdot 10^8$	$(2.7 \pm 0.2) \cdot 10^{10}$	17.5 ± 1.6	1.25[69] 4.27[70]
Succinic	$(1.2 \pm 0.1) \cdot 10^7$	$(7.6 \pm 0.6) \cdot 10^{10}$	21.4 ± 1.8	4.21[69] 5.63[71]
Maleic	$(1.8 \pm 0.1) \cdot 10^7$	$(7.0 \pm 0.3) \cdot 10^{11}$	25.8 ± 1.0	1.94[72] 6.22[72]
Adipic	$(8.0 \pm 0.8) \cdot 10^6$	$(8.7 \pm 0.8) \cdot 10^{11}$	28.3 ± 2.7	4.43[73] 5.41[69]

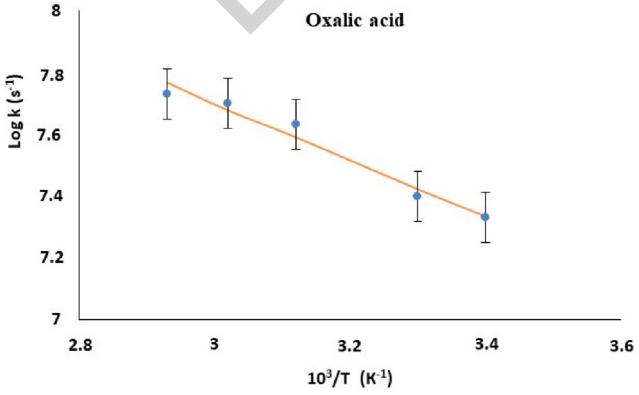

Figure 2. The Eyring plot of the intermolecular rate constant exchange for 3,6-di-tert-butyl-2-hydroxyphenoxyl with oxalic acid in toluene.

Additionally, a correlation has been found between the kinetic and activation parameters and the thermodynamic acidity of the acids under investigation.

The difference in the values of the entropy of activation $\Delta S^{\#}$ between maleic and succinic acids is attributed to the specific structural and electronic features of maleic acid that facilitate effective preorganization of the reacting system. The double bond in maleic acid fixes the carboxyl groups in a *cis*-conformation, promoting the formation of a stable intramolecular hydrogen bond. This results in a rigidly organized geometry already present in the ground state. Such preorganization significantly reduces the additional entropy loss that would otherwise occur during the formation of the transition complex required for synchronous double proton transfer. Moreover, the electronic influence of the double bond (inductive and conjugative effects) may contribute to the redistribution of electron density within the carboxyl groups, thereby facilitating the activation of proton exchange.

Thus, despite having a higher enthalpic barrier, maleic acid exhibits a higher rate of proton exchange due to its internal structural preorganization.

Note that the relatively small values of pre-exponential coefficients of Arrhenius parameters shown in Table 1 are well explained within the framework of the Eyring equation.[40]

$$k_{exch} = \frac{k_B T}{h}\exp\left(\frac{-\cdot G^{\#}}{RT}\right) = \frac{k_B T}{h}\exp\left(\frac{-\cdot H^{\#}}{RT} + \frac{\cdot S^{\#}}{R}\right) \quad (2)$$

Using the Eyring equation allows us to determine the activation parameters of proton exchange presented in **Table 2**.

The data presented in Table 2 indicate that, within experimental error, the Gibbs free energy of activation for the intermolecular double proton exchange remains nearly constant and is practically independent of the acid structure. The IPE process is endothermic, with the enthalpy of activation increasing as the size of the acid increases. As the system approaches the transition state, the degree of order increases, as evidenced by the negative values of $\Delta S^{\#}$. This is likely associated with the formation of a cyclic complex between the reactants. However, this trend becomes less pronounced as the carbon chain length increases from oxalic to adipic acid.

The decrease in entropy of activation ($\Delta S^{\#}$) with increasing acid size can be explained by several molecular factors related to the geometry and dynamics of the molecules in the transition state. First, as the carbon chain length of the dicarboxylic acids increases, so does the conformational flexibility of the molecule in

Table 2. Activation parameters of proton exchange of 3,6-di-tert-butyl-2-hydroxyphenoxyl with acids. Solvent–toluene.

Acid	$\Delta G^{\#}$ [$kJ \cdot mol^{-1}$]	$\Delta H^{\#}$ [$kJ \cdot mol^{-1}$]	$\Delta S^{\#}$ [$J \cdot K^{-1} \cdot mol^{-1}$]
Oxalic	30.7± 0.1	14.9 ± 1.6	-53.9 ± 0.1
Succinic	32.6 ± 1.9	18.8 ± 1.9	-45.4 ± 0.8
Maleic	31.1 ± 0.1	23.3 ± 1.0	-26.5 ± 3.4
Adipic	33.0 ± 3.6	25.6 ± 2.7	-25.3 ± 7.9

Table 3. Experimentally obtained kinetic parameters of 3,6-di-tert-butyl-2-hydroxyphenoxyl–acid systems.

Acid	k/k_s	Log A [s^{-1}]	Δm [a.m.u]	2a [Å]	E_m [kJ · mol^{-1}]	E_d [kJ · mol^{-1}]	E_{obs} [kJ · mol^{-1}]
Oxalic	1.4	12.6	2	0.5	13	17.5	30.5
Succinic	1.5	12.6	2	0.5	10.8	21.4	32.1
Maleic	1.7	12.6	2	0.5	5.5	25.8	31.3
Adipic	1.8	12.6	2	0.5	5.2	28.3	33.4

its ground state. However, in the transition state, a precise orientation of the carboxyl groups is required for efficient proton transfer, leading to an entropic loss due to the restriction of possible conformations. Thus, more flexible molecules experience a greater entropy loss upon transitioning into the ordered transition state.

Second, structural features, such as the distance between reactive groups, play a key role. In maleic acid (*cis*-configuration), the distance between the carboxyl groups is minimal, which facilitates proton transfer with fewer structural rearrangements and, consequently, a smaller entropy loss. In contrast, for succinic and adipic acids (*trans* and linear configurations), achieving the required geometry involves more pronounced reorganization, accompanied by a greater decrease in entropy.

The obtained kinetic data were analyzed using the Bell–Limbach theory[41] based on a 1D model with a double-well potential.[42–45] The Bell–Limbach model describes the kinetic and thermodynamic aspects of proton transfer and activation processes, including quantum tunneling effects and hydrogen bond interactions. The obtained parameters are summarized in **Table 3**. As initial values, the following were used: Log A = 12.6, barrier width 2a = 0.5 Å (estimated from theoretical results), and the effective tunneling mass m = 2 (in atomic units).

In toluene, the experimentally accessible temperature range lies at the center of the concave region of the Arrhenius curve

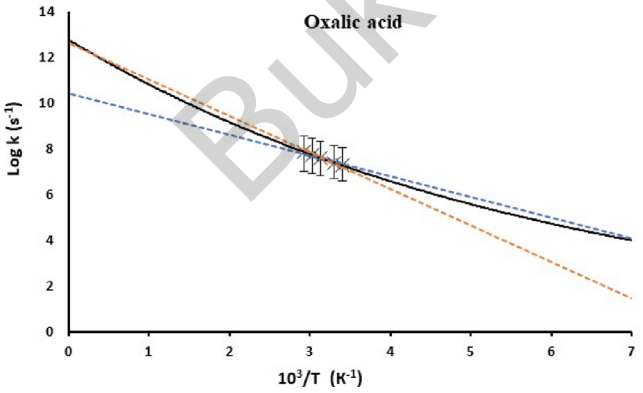

Figure 3. Arrhenius curve of double H transfer of 3,6-di-tert-butyl-2-hydroxyphenoxyl- oxalic acid system in toluene calculated according to the Bell–Limbach tunneling model. Minimum energy for tunneling to occur $E_m = 13$ kJ · mol^{-1}, barrier heights $E_d = 17.5$ kJ · mol^{-1}, and tunneling masses $m_H = 2 + \Delta m$. Barrier width 2_{a_u}. The blue dashed lines represent the experimental data, while the orange dashed lines correspond to theoretical values calculated within the framework of transition state theory (TST) at 298 K. The calculations were performed using a pre-exponential factor of kT/h = $10^{12.6}$ s^{-1}.

(**Figure 3**). The Arrhenius plots for the IPE reaction between the radical and the acids exhibit a similar shape to those observed for hydrogen transfer in the unsubstituted 2-hydroxyphenoxyl radical and the substituted 3,6-di-tert-butyl-2-hydroxyphenoxyl radical.[42]

Hydrogen transfer in systems with hydrogen bonds is a multidimensional problem involving multiple factors that contribute to the reaction coordinate. Experimentally identifying and accounting for these contributions is challenging. The process may be related to the structure of the forming transition complex, the compression of hydrogen bonds within the complex, and the influence of intramolecular proton transfer within the radical.

In this model, key parameters include the tunneling energy, E_m, and the height of the energy barrier, E_d. Analysis of the kinetic data shows that, in some of the studied systems, the value of E_m exceeds that of E_d. With increasing acid chain length, this difference also increases, which may be associated with molecular skeleton reorganization leading to closer proximity of the radical–acid complex fragments involved in hydrogen transfer.

A slight deviation from linearity in the Arrhenius plot is a characteristic feature and direct evidence of a significant contribution of quantum mechanical tunneling to the overall reaction rate. In contrast to a purely thermally activated process, where the Arrhenius dependence is strictly linear, the presence of tunneling results in a concave curvature of the plot. This indicates that the reaction rate decreases more slowly with decreasing temperature than would be predicted by thermal activation alone. This observation is consistent with the theoretical predictions of the Bell–Limbach model and confirms the importance of accounting for tunneling effects in this system.

As is known, the nature of the solvent can significantly affect the reaction rate. This is especially evident in environments with pronounced properties for intermolecular binding of reagents. Analysis of changes in reactivity in relatively indifferent environments can provide important information about the reaction mechanism and the intermediate states formed.

Analysis of the kinetic parameters of the proton exchange reaction in a toluene medium reveals higher values than those obtained earlier in a dioxane medium. In this case, the geometry of the cyclic complex necessary for a favorable exchange reaction can be distorted, which directly affects the overall reaction rate while leveling the effect of the medium on the entire mechanism of the process, which is complex.

Numerous experimental data on fast proton exchange between radical and various OH acids indicate that an indispensable condition for such an intermolecular reaction is, in all likelihood, the obligatory formation of a cyclic complex between the

reaction partners due to a hydrogen bond. The stage of intracomplex proton transfer along the hydrogen bond chain will limit the rate of IPE. It is also clear that the acidity of the reaction partners will determine the symmetry of the transient cyclic complex.

2.2. Computational Data

Calculations based on density functional theory (DFT) were carried out to study the mechanisms of the above-described IPE reactions. Geometry optimization, search for transition, and vibrational analysis were carried out with the B3LYP functional[46–48] and the 6−31 + G(d,p) basis set.[49] Due to the size of the complex, all optimizations were performed in the gas phase and refined in solution using the polarizable continuum solvation model (PCM)[50] and conductor-like polarizable continuum model (CPCM)[51] for all solvents. All calculations were done using the Gaussian 16 and Firefly software packages.[52–55] The supporting information shows optimized geometries, energies, and vibrational frequencies for all species for which we performed calculations.

Figure 4a shows a fragment of the studied radical–acid system.

For all the studied systems, the optimized structures corresponding to the initial, final, and transition states and the energy characteristics of the process under consideration were calculated. Table 2 in the supporting information provides the internuclear distances within the cyclic complexes of the studied systems, calculated for both the gas phase and toluene solution. Many studies have been devoted to quantum chemical calculations of the properties of oxalic,[56,57] succinic,[58] maleic,[59] and adipic[60] acids, which allowed us to understand their molecular structure and reactivity better. We calculated the intrinsic reaction coordinate (IRC) for all the studied systems to model the reaction mechanism and obtained the PES profiles. Figure 4b shows the PES profile of the Rad–OxA system.

Figure 4 presents the energy characteristics of the radical complexes with acids corresponding to the process's initial, final, and intermediate states under consideration in the gas phase and toluene. Analysis of internuclear distances in the gas phase of the Rad–OxA system presented in Figure 4b shows that during the formation of complexes, the length of the hydrogen bridges (O1–O2) and (O3–O4) changes within the range from 2.60 Å to 2.73 Å and vice versa in the initial and final states, respectively, in the gas phase, whereas in toluene, the distance (O1–O2) decreases to 2.59 Å, and the distance (O3–O4), on the contrary, increases to 2.75 Å in the initial state and vice versa for the final state. These changes are characteristic of systems with cooperative hydrogen bonds in which the compression of one bond leads to the compression of the other.[16]

Moreover, this process is coordinated. Intermolecular hydrogen bonds are compressed simultaneously, which we observe in the transition state for the bond (O1—O2) to 2.41 Å, and for the bond (O3—O4) to 2.42 Å in the gas phase, and (O1—O2) to 2.43 Å and for the bond (O3—O4) to 2.44 Å in toluene. The bond (O1—O2) with radical oxygen is slightly compressed, while the other bond (O—O4) is stretched.

Analysis of distances in the homologous series of acids showed a slight decrease in the lengths of hydrogen bridges (O1–O2) and (O3–O4) in the series of dicarboxylic acids with an increase in the chain length. A similar picture is characteristic of the transition state, in which the lengths of the hydrogen bridges (O1–O2) and (O3–O4) in the cyclic fragment of the intermolecular complexes decrease from 2.41 Å to 2.39 Å in the gas phase and from 2.43 Å to 2.38 Å in a toluene medium with an increase in the number of carbon atoms in the acid molecule.

Solvation of the complex leads to a slight increase in the distance between the radical and the acid, while the O—H bond is compressed in the molecules of the radical and the acid.

In the transition state, the structure of the intermolecular cyclic complex of the acid with the radical changes. If, in the initial and final states, a flat structure of the complex is observed, then

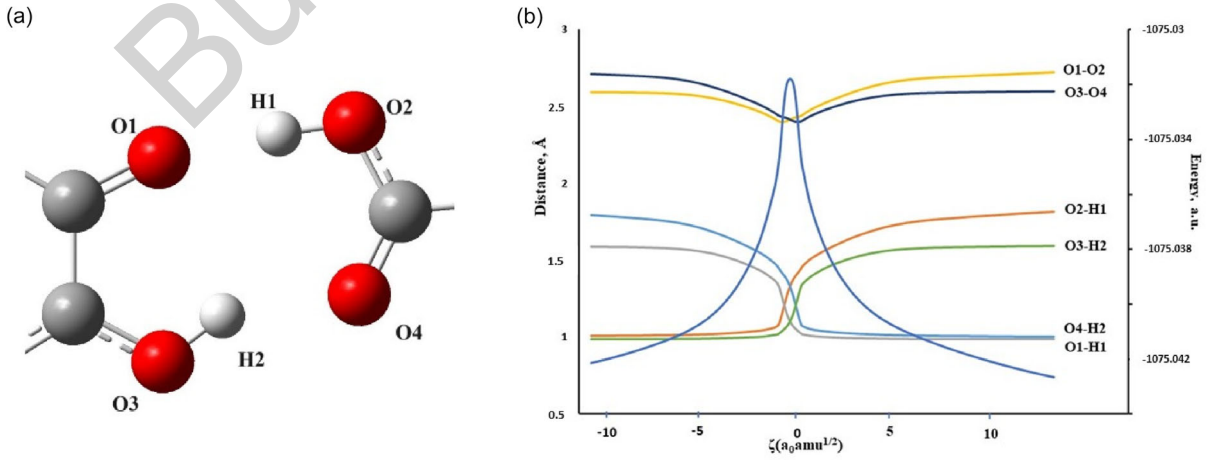

Figure 4. a) A fragment of the radical–acid system. b) Changes in the distance between bonds in the Rad–OxA system. The distances between the oxygen–oxygen (O1–O2), (O3–O4); oxygen–hydrogen (O2–H1), (O3–H2) and oxygen–hydrogen (O1–H1) (O4–H2) bonds are shown here. Here, O2, O3 are proton donors, and O1, O4 are proton acceptors.

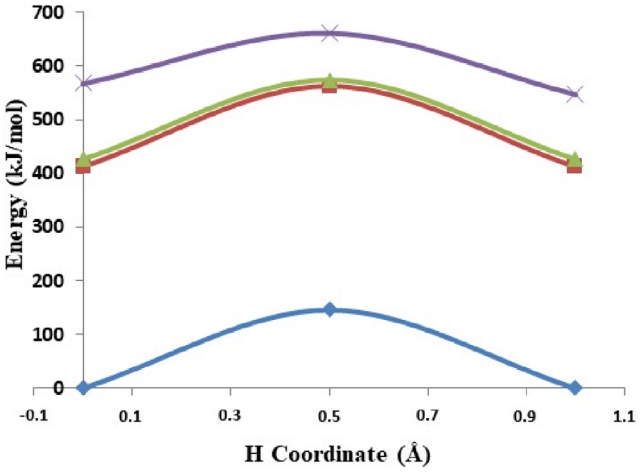

Figure 5. Electron-adiabatic potential energy curves as a function of the linearly interpolated coordinate for Rad–OxA systems. The blue curve represents the adiabatic energies of the ground state, the red curve is the first excited state, the green curve is the second excited state, and the violet curve is the third excited state, respectively, calculated by the CASSCF/XMCQDPT method.

in the transition state, there is a distortion of the structure and the dihedral angle of the fragment (O1–O2–O3–O4) in the studied series of acids from 39° (for oxalic acid) to 32° (for adipic acid) in the gas phase, and from 39° to 33°, respectively, in a toluene medium.

To account for electron correlation within the active space, a multiconfigurational self-consistent field calculation was performed using the complete active space (CAS) method, followed by dynamic energy correction with the XMCQDPT method. The XMCQDPT method represents a novel approach to second-order multistate multireference perturbation theory, as developed by Granovsky (**Figure 5**).[61–64]

The CAS active space comprised one active electron distributed across three active orbitals (CAS(1,3)), which corresponds to the description of the system's valence electron distribution. The graphical unitary group approach (GUGA-CI) method, as implemented in the Firefly 8.2.0 program,[54] was employed for the calculation.

The CAS(1,3) active space was selected to explicitly account for the unpaired electron localized on the π^*-orbital of the semiquinone radical and the two π-orbitals of the quinoid fragment. This selection ensures a correct description of the spin density and electron density delocalization, which is critical for understanding the electronic structure of the system. Expansion to larger active spaces would not yield a significant improvement in the results. The GUGA-CI method, as implemented in the Firefly 8.2.0 program, provides an accurate description of electron correlation at a reasonable computational cost, which is supported by the consistency of the results with other methods.

Figure 5 illustrates the changes in electronic energy of various states as a function of the linearly interpolated reaction coordinate. Analysis of the obtained curves reveals that the singly occupied molecular orbital (SOMO) is localized on the radical, while the ground electronic state remains unchanged throughout

Table 4. Calculated Gibbs free energy of activation ($\Delta G^{\#}$) for IPE between semiquinone radical and dicarboxylic acids in toluene (DFT/CPCM calculations).

Acid	Oxalic	Succinic	Maleic	Adipic
$\Delta G^{\#}$ [kJ · mol^{-1}]	22.0	21.5	21.2	17.9

the reaction process. Only a redistribution of charges on the hydrogen atoms is observed. Quasidegeneracies between the ground state and excited states were not detected, indicating the feasibility of describing the model within the framework of DFT, considering only the ground state.

Quantum chemical calculations at the DFT/CPCM level of theory, performed using the Gaussian software package, were employed to determine the Gibbs free energy of activation ($\Delta G^{\#}$) for the intermolecular proton transfer reaction between a series of dicarboxylic acids and the semiquinone radical in toluene (see **Table 4**). These calculations show a decrease in the activation energy ($\Delta G^{\#}$) with increasing length of the aliphatic chain, reaching the lowest value for adipic acid.

This trend indicates that the molecular flexibility of the acid facilitates a reduction in the energetic barrier for proton transfer. Longer and more flexible chains, such as those found in adipic acid, can more readily adapt to the geometry of the transition state, thereby reducing steric and conformational constraints.

It should be noted that DFT/CPCM calculations, particularly those utilizing the B3LYP functional, are known to systematically underestimate the heights of energy barriers. The observed underestimation of the theoretical ($\Delta G^{\#}$) values relative to the experimental activation energies (see Table 1) falls within the typical error range of the method ($\pm$13–17 kJ mol^{-1}). Nevertheless, the calculations qualitatively reproduce the trend in reactivity as a function of chain length.

It is important to emphasize that the calculations describe only the elementary proton transfer step, whereas the experimental kinetic data may reflect a combined process that includes diffusional contributions. The discrepancy between the theoretical trend (decreasing $\Delta G^{\#}$ with increasing chain length) and the experimental dependence of activation energy suggests a shift toward a diffusion-controlled regime for more hydrophobic, long-chain acids such as adipic acid. In contrast, better agreement between theory and experiment is observed for short-chain acids (oxalic and succinic acids), confirming the adequacy of the CPCM model in describing the intrinsic proton transfer step in a nonpolar medium.

The supporting information Table 3 presents the charges on atoms in the cyclic complexes of the studied systems, obtained for the gas phase and toluene. **Figure 6**a shows the charge dynamics on reference atoms during proton exchange.

Comparison of the CHELPG charges of the radical–oxalic acid system on the oxygen atoms of the radical (O1 and O3) and the acid (O2 and O4) in the initial, final, and transition states, as well as on the hydrogen atoms (H1 and H2) shows that the charge dynamics on the oxygen atoms does not undergo significant changes. The most considerable charge changes occur on the

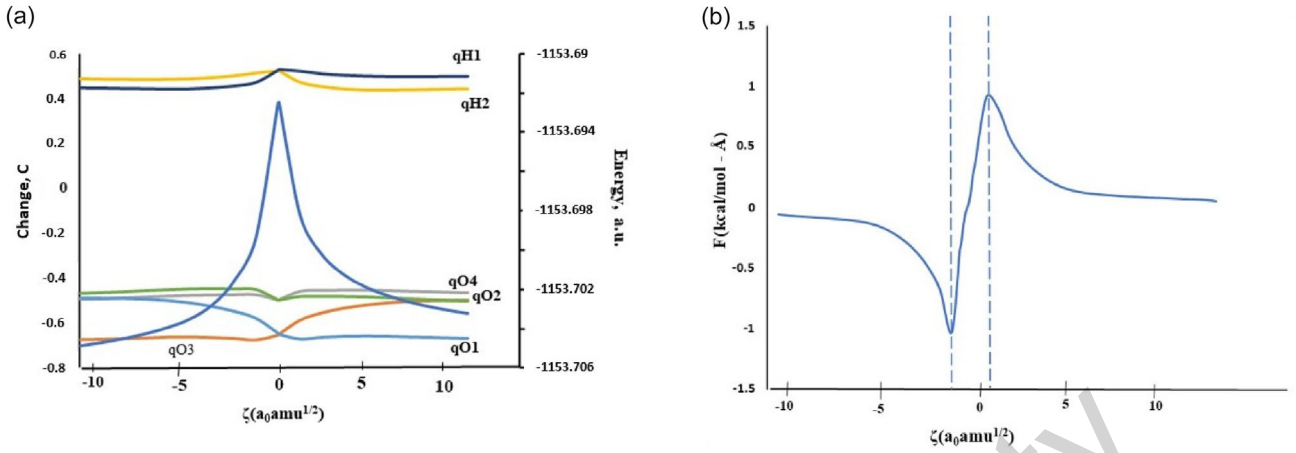

Figure 6. Reaction profiles for the radical–oxalic acid system. a) Potential energy along the internal coordinate of reaction, calculated using the B3LYP 6-31 + G(d,p) method. b) Charge distribution along the reaction internal coordinate. Reaction force profile. The dashed lines indicate the minimum and maximum of the reaction force, respectively.

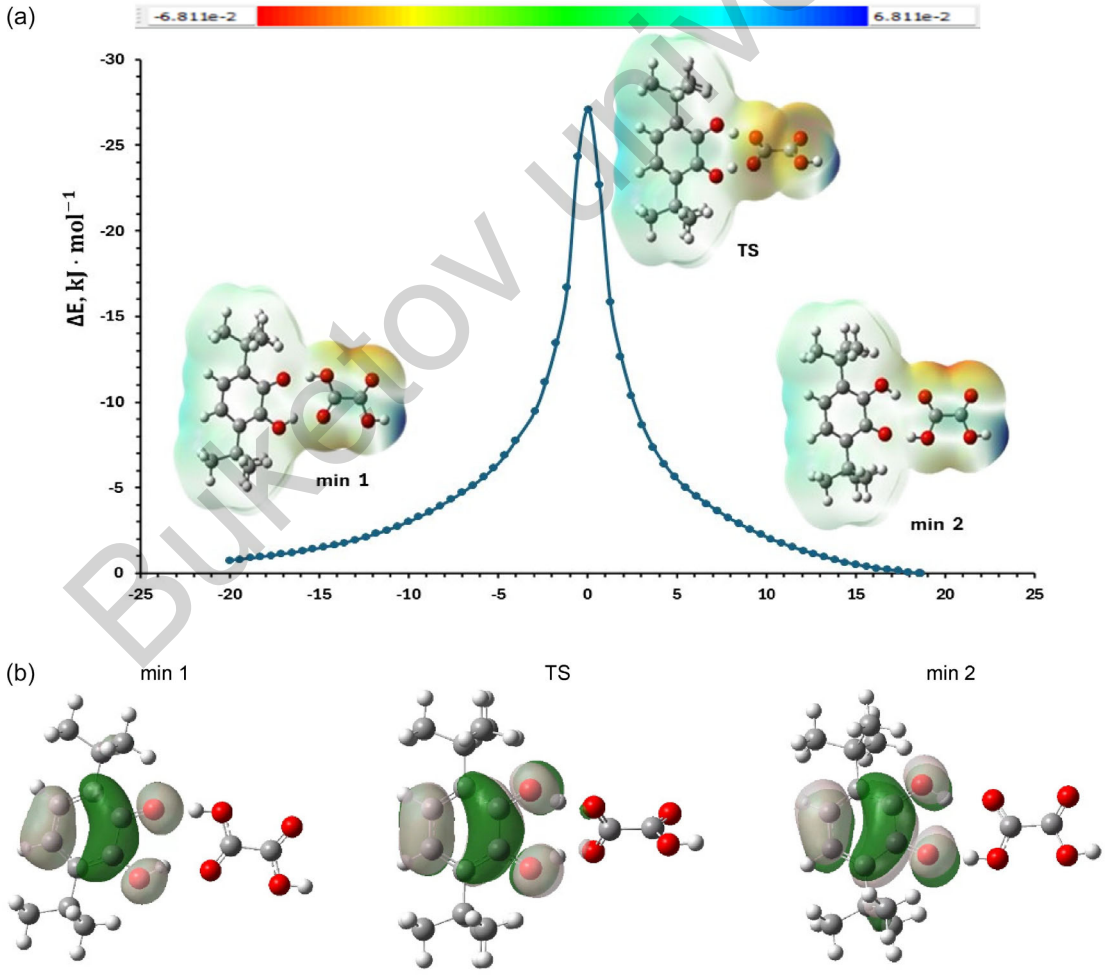

Figure 7. a) ESP maps for the adiabatic ground state, the initial state (minimum 1), the transition state, and the final (minimum 2) along the reaction path for the hydrogen-transferring positions in the radical–oxalic acid system in toluene. Negatively and positively charged regions are shown in red and blue, respectively. b) SOMO for the ground electronic states for the Rad–OxA system in toluene, for the initial state (min 1), transition state (TS), and final state (min 2) positions of the transferring hydrogens.

radical centers (O1 and O3), while they are insignificant on the oxygen atoms (O2 and O4). A similar picture, presented in works,[65–68] is characteristic of the phenol–phenoxyl, toluene–benzyl, and aroxyl systems, from which it can be assumed that these dynamics are characteristic of processes involving a hydrogen atom. For the Rad–OxA system (Figure 6b), since the configurations of the initial and final are almost identical, we see consistent electronic activity with the onset of the reaction. Immediately before entering the transition state region, the reaction force drops sharply to a minimum position. Then, it increases sharply toward the transition state, where the force disappears along the reaction coordinate. This behavior can be further analyzed by studying the changes in the distance between the O—O and O—H bonds along the reaction coordinate (Figure 6b). An initiating increase in the distance between the O2—H1 and O3—H2 bonds and a significant decrease in the distance between the O4—H2 and O1—H1 bonds accompanies the sharp drop in the reaction force.

In contrast, the distance between the O1—O2 and O3—O4 bonds does not change significantly. It is at this range that a double proton transfer occurs. Namely, the O2—H1 and O3—H2 bonds are broken, but the O4—H2 and O1—H1 bonds are formed.

Synchronous destruction and bond formation appear at the dividing lines of extreme forces. Structural and electronic reorganizations occur throughout the reaction path. Overall, the subtle charge redistribution and structural changes reveal the mechanism of the concerted DPT reaction.

Analysis of the evolution of electrostatic potential (ESP) maps along the IRC indicates that the proton exchange process in the investigated complex is accompanied by a redistribution of electron density and, consequently, a change in electrostatic interactions. The transition state is characterized by a specific ESP distribution, reflecting the dynamics of the charge transfer process. The obtained data underscore the crucial role of electrostatic factors in determining the energy barrier and thermodynamic favorability of the proton exchange reaction in the studied system (**Figure 7**a).

Analysis of the spin density distribution of the initial (min 1), final (min 2), and transition states during the transfer showed that in the initial and final states, the spin density is distributed in the aromatic ring, oxygen atoms, and partly on the hydrogen atom of the hydroxyl group of the radical. In contrast, in the transition state, the spin density is partly distributed on the transferred hydrogen atoms (Figure 7b). This is consistent with the picture characteristic of the process observed in the phenoxyl–phenol system and interpreted as the hydrogen atom transfer (HAT) mechanism.[68]

The observed changes in the shape and localization of the SOMO during the proton exchange reaction demonstrate the dynamic nature of the electronic structure during the elementary act of chemical transformation. The SOMO of the transition state is characterized as predominantly localized on the semiquinone radical fragment, with a potentially negligible degree of delocalization on the oxalic acid fragment. Shifts in the preferential localization of SOMO from initial state (min 1) to final state (min 2) indicate which fragment of the molecular complex carries the primary unpaired electron density upon completion of the proton exchange process.

3. Conclusion

This work demonstrated the possibility of applying dynamic ESR spectroscopy to protolytic processes involving oxyphenoxyl radicals, such as 3,6-di-tert-butyl-2-hydroxyphenoxyl. Due to this method's time resolution, dynamic changes during the reaction can be observed experimentally. Qualitative interpretation of the experimental Arrhenius plots using the Bell–Limbach model gives some insight into the reaction mechanism, which requires further theoretical studies.

A theoretical study of the energy profiles of the double proton transfer reaction in oxyphenoxyl radical–dicarboxylic acid systems using the B3LYP 6-31 + G(d,p) DFT showed that taking into account dispersion and correlation effects is necessary to reproduce the experimental activation energies. From the calculated energies and spin densities along the energetically lower reaction, we concluded that the HAT mechanism is present in the studied systems. A detailed study of the reaction pathway using the IRC procedure confirmed that the DPT reaction occurs when two molecules are combined. At the same time, the hydrogen bonding pattern remains virtually unchanged.

Conflict of Interest

The authors declare no conflict of interest.

Data Availability Statement

The data that support the findings of this study are available in the supplementary material of this article.

Keywords: 3,6-di-*tert*-butyl-2-hydroxyphenoxyl · bloch equation · density functional theories · proton exchange reactions · transition states

[1] J. Saha, S. Banerjee, S. Malo, A. K. Das, I. A. Das, *Exp. Theor. Stud. Chem. Eur. J.* **2024**, *30*, e202304009.
[2] P. Walter, O. Hübner, E. Kaifer, H.-J. Himmel, *Chem. Eur. J.* **2021**, *27*, 11943.
[3] R. Kumar, N. Vaval, *ChemPhysChem* **2022**, *24*, e202200340.
[4] J. Torić, A. Karković Marković, S. Mustać, A. Pulitika, C. Jakobušić Brala, V. Pilepić, *Int. J. Mol. Sci.* **2024**, *25*, 6341.
[5] Y. Litman, J. O. Richardson, T. Kumagai, M. Rossi, *J. Am. Chem. Soc.* **2019**, *141*, 2526.
[6] R. Tyburski, T. Liu, S. D. Glover, *J. Am. Chem. Soc.* **2021**, *143*, 560.
[7] H.-H. Limbach. Proton Tautomerism in Systems of Increasing Complexity: Examples from Organic Molecules to Enzymes in L. Antonov, *Ed. Tautomerism. Concepts And Applications In Science And Technology*, (Eds.: G. S. Denisov, I.G. Shenderovich, P. M. Tolstoy) Wiley-VCH, Weinheim **2016**, Chapter 14, pp. 329–372.
[8] S. Hammes-Schiffer, *J. Am. Chem. Soc.* **2015**, *137*, 8860.
[9] Y.-H. Cheng, Y.-C. Zhu, W. Kang, X.-Z. Li, W. Fang, *J. Chem. Phys.* **2022**, *156*, 124304.
[10] S. Gholami, M. Aarabi, S. J. Grabowski, *ChemPhysChem* **2024**, *25*, e202300849.

[11] J. W. Darcy, B. Koronkiewicz, G. A. Parada, J. M. Mayer, *Acc. Chem. Res.* **2018**, *51*, 2391.
[12] Y.-S. Wang, K.-L. Shen, S. D. Chao, *Chin. J. Phys.* **2017**, *55*, 719.
[13] H. Liu, J. Cao, W. Bian, *Front. Chem.* **2019**, *7*, 676.
[14] T. Yoshida, K. Hirozumi, M. Harada, S. Hitaoka, H. Chuman, *J. Org. Chem.* **2011**, *76*, 4564.
[15] B. Kizior, M. Michalczyk, J. J. Panek, W. Zierkiewicz, A. Jezierska, *Int. J. Mol. Sci.* **2023**, *24*, 1542.
[16] H.-H. Limbach, S. Baumgärtner, R. Franke, F. Männle, G. Scherer, G. S. Denisov, *Molecules* **2021**, *26*, 4373.
[17] D. Gerritzen, H.-H. Limbach, *J. Am. Chem. Soc.* **1984**, *106*, 869.
[18] J. M. Lopez, F. Männle, I. Wawer, G. Buntkowsky, H.-H. Limbach, *Phys. Chem. Chem. Phys.* **2007**, *9*, 4498.
[19] V. Torres, J.-M. Lopez, U. Langer, G. Buntkowsky, H.-M. Vieth, J. Elguero, H.-H. Limbach, *Z. Phys. Chem.* **2012**, *226*, 1125.
[20] B. Koeppe, P. M. Tolstoy, J. Guo, G. S. Denisov, H.-H. Limbach, *J. Phys. Chem. B.* **2021**, *125*, 5874.
[21] J. Quintero-Saume, D. A. M. RinconDörr, M. Dörr, M. C. Daza, *Phys. Chem. Chem. Phys.* **2017**, *19*, 26179.
[22] X.-B. Wang, Q. Fu, J. Yang, *J. Phys. Chem. A* **2010**, *114*, 9083.
[23] N. O. Druzhkov, E. N. Egorova, M. V. Arsen'ev, E. V. Baranov, V. K. Cherkasov, *Russ. Chem. Bull., Int. Ed.* **2016**, *65*, 2855.
[24] A. S. Masalimov, S. N. Nikolsky, A. A. Khodak, A. I. Prokofiev, Z. M. Muldakhmetov, *Theo. Exp. Chem.* **1991**, *27*, 244.
[25] X. Wang, Y. Wang, H. Li, *Asian J. Org. Chem.* **2023**, *12*, e202300475.
[26] J. Bachle, F. Gonia, G. Grampp, *Phys. Chem. Chem. Phys.* **2015**, *17*, 27204.
[27] R. Stösser, W. Herrmann, U. Marx, A. Brückner, *J. Phys. Chem. A.* **2011**, *115*, 2939.
[28] A. S. Masalimov, S. N. Nikolskii, P. I. Dmitriev, A. I. Prokofiev, Z. M. Muldakhmetov, *Bull. Acad. Sci. USSR, Div. Chem. Sci.* **1991**, *40*, 53.
[29] S. N. Nikolskiy, F. Z. Abilkanova, A. S. Golovenko, I. A. Pustolaikina, A. S. Masalimov, *Bull. Univ. Karaganda Chem.* **2020**, *98*, 35.
[30] A. S. Masalimov, A. A. Tur, S. N. Nikolskiy, *Theor. Exp. Chem.* **2016**, *52*, 57.
[31] I. L. Stadnik, F. Zh. Abilkanova, Ye. V. Kudryavtseva, S. N. Nikolskiy, A. S. Masalimov, *Bull. Univ. Karaganda Chem.* **2022**, *106*, 69.
[32] A. F. Kurmanova, F. Zh. Abilkanova, A. S. Rakhimzhanova, I. A. Pustolaikina, *Eurasian J. Chem.* **2022**, *106*, 43.
[33] A. F. Kurmanova, F. Zh. Abilkanova, I. A. Pustolaikina, S. N. Nikolskiy, *Eurasian J. Chem.* **2023**, *111*, 143.
[34] Z. G. Keolopile, M. R. Ryder, M. Gutowski, *J. Phys. Chem. A* **2014**, *118*, 7385.
[35] A. J. Mota, E. Colacio, J.-P. Costes, F. Dahan, *Polyhedron* **2013**, *63*, 127.
[36] T. H. Willke, K.-D. Vorlop, *Appl. Microbiol. Biotechnol.* **2004**, *66*, 131.
[37] E. M. S. Maçôas, R. Fausto, J. Lundell, M. Pettersson, L. Khriachtchev, M. Räsänen, *J. Phys. Chem. A* **2001**, *105*, 3922.
[38] U. Schuchardt, D. Cardoso, R. Sercheli, R. Pereira, R. S. Cruz, M. C. Guerreiro, D. Mandelli, E. V. Spinace, E. L. Pires, *Appl. Catal. A.* **2001**, *211*, 1.
[39] S. N. Nikolskiy, *Bull. L. N. Gumilyov Eurasian Natl. Univ., Chem.* **2007**, *60*, 160.
[40] S. Hammes-Schiffer, *ChemPhysChem* **2002**, *3*, 33.
[41] R. P. Bell, *The Tunnel Effect in Chemistry*, (Hon. Research Professor of Physical Chemistry University of Leeds) Originally published by Chapman and Hall in **1980**.
[42] H.-H. Limbach, K. B. Schowen, R. L. Schowen, *J. Phys. Org. Chem.* **2010**, *23*, 586.
[43] H.-H. Limbach, J. M. Lopez, A. Kohen, *Philos. Trans. R. Soc. B* **2006**, *361*, 1399.
[44] H.-H. Limbach. in *Hydrogen Transfer Reactions*, Vol. 1&2 (Eds.: J. T. Hynes, J. Klinman, H.-H. Limbach, R. L. Schowen), VCH, Weinheim, Germany **2007**; Chapter 6, pp. 135–221.
[45] J. M. Lopez, F. Maënnle, I. Wawer, G. Buntkowsky, H.-H. Limbach, *Phys. Chem. Chem. Phys.* **2007**, *9*, 4498.
[46] A. D. Becke, *J. Chem. Phys.* **1993**, *98*, 5648.
[47] P. J. Stephens, F. J. Devlin, C. F. Chabalowski, M. J. Frisch, *J. Phys. Chem.* **1994**, *98*, 11623.
[48] S. Grimme, J. Antony, S. Ehrlich, H. Krieg, *J. Chem. Phys.* **2010**, *132*, 154104.
[49] P. C. Hariharan, J. A. Pople, *Theor. Chim. Acta* **1973**, *28*, 213.
[50] J. Tomasi, B. Mennucci, R. Cammi, *Chem. Rev.* **2005**, *105*, 2999.
[51] G. Scalmani, M. J. Frisch, *J. Chem. Phys.* **2010**, *132*, 114110.
[52] M. J. Frisch, G. W. Trucks, *Gaussian 16, Revision A.03*: Gaussian, Inc., Wallingford, CT **2016**.
[53] R. Dennington, T. A. Keith, J. M. Millam, *GaussView, Version 6.1*, Semichem Inc., Shawnee Mission, KS **2016**.
[54] A. A. Granovsky, Version 8; Firefly icon and logo original design by Lyndsey Vernon, *Chemistry*, University of Liverpool **2020**.
[55] M. W. Schmidt, K. K. Baldridge, J. A. Boatz, S. T. Elbert, M. S. Gordon, J. H. Jensen, S. Koseki, N. Matsunaga, K. A. Nguyen, S. Su, T. L. Windus, M. Dupuis, J. A. Montgomery, J. Comput, *Chem.* **1993**, *14*, 1347.
[56] J.-G. Chang, H.-T. Chen, S. Xu, M. C. Lin, *J. Phys. Chem. A* **2007**, *13*, 6789.
[57] K. K. Tadi, R. V. Motghare, *J. Chem. Sci.* **2013**, *125*, 413.
[58] A. Sener, M. M. Kadiata, L. Ladrière, W. J. Malaisse, *Endocrine* **1997**, *7*, 151.
[59] M. Zhang, Z. Huang, Q. Yan, *Adv. Mater. Res.* **2009**, *79–82*, 1193.
[60] Y. Wen, X. Wang, H. Wei, B. Li, P. Jin, L. Li, *Green Chem.* **2012**, *14*, 2868.
[61] A. A. Granovsky, *J. Chem. Phys.* **2011**, *134*, 214113.
[62] R. Parr, W. Yang, *Density-Functional Theory Of Atoms And Molecules*, Oxford University Press, New York **1989**, p. 352.
[63] P. Geerlings, F. de Proft, W. Langenaeker, *Chem. Rev.* **2003**, *103*, 1793.
[64] R. G. Parr, R. A. Donnelly, M. Levy, W. E. Palke, *J. Chem. Phys.* **1978**, *68*, 3801.
[65] J. M. Mayer, D. A. Hrovat, L. Jennie, *J. Am. Chem. Soc.* **2002**, *124*, 11142.
[66] A. Sirjoosingh, S. Hammes-Schiffer, *J. Phys. Chem. A.* **2011**, *115*, 2367.
[67] J. H. Skone, A. V. Soudackov, S. Hammes-Schiffer, *J. Am. Chem. Soc.* **2006**, *128*, 16655.
[68] J. Böchle, M. Marković, A.-M. Kelterer, G. Grampp, *ChemPhysChem* **2017**, *18*, 2932.
[69] W. M. Haynes. *CRC Handbook Of Chemistry And Physics 96th Edition A Ready-Reference Book Of Chemical And Physical Data*, (Eds.: Scientist Emeritus National Institute of Standards and Technology Associate Eds David R. Lide, Ph.D. Former Director, Standard Reference Data National Institute of Standards and Technology Thomas J. Bruno, Ph.D. Group Leader National Institute of Standards and Technology) Wiley-VCH, Weinheim **2015**, Chapter 14, pp. 329–372.
[70] https://surl.li/lofbkl.
[71] https://pubchem.ncbi.nlm.nih.gov/compound/1110#section=Refractive-Index.
[72] https://pubchem.ncbi.nlm.nih.gov/compound/444266#section=Heat-of-Combustion.
[73] https://en.wikipedia.org/wiki/Adipic_acid.

Manuscript received: May 6, 2025
Revised manuscript received: August 7, 2025
Version of record online: August 21, 2025